Powder Technology 412 (2022) 117982

Contents lists available at ScienceDirect

Powder Technology

journal homepage: www.journals.elsevier.com/powder-technology

# Application of the Rosin-Rammler function to describe quartz sandstone particle size distribution produced by high-pressure gas rapid unloading at different infiltration pressure

Genghao Zhang [a], Yongbo Fan [b], Renshu Yang [a,*], Shihai Li [b]

[a] School of Civil and Resource Engineering, University of Science and Technology Beijing, Beijing 100083, China
[b] Key Laboratory for Mechanics in Fluid Solid Coupling Systems, Institute of Mechanics, Chinese Academy of Sciences, Beijing 100190, China

## HIGHLIGHTS

- Pulverize quartz sandstone using high-pressure gas rapid unloading.
- The infiltration pressure significantly affects the quartz sandstone pulverization.
- Correlating the infiltration pressure with the R-R function.
- Finally, the R-R function can depict PSD obtained at various infiltration pressures.

## GRAPHICAL ABSTRACT

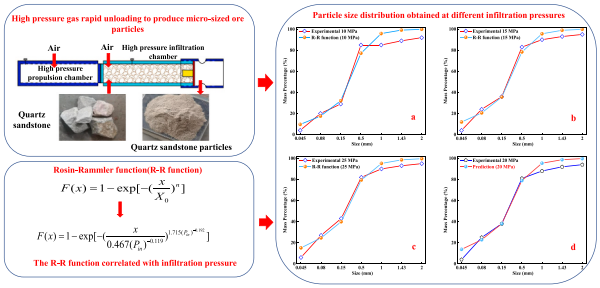


This paper correlates the infiltration with the R-R function to describe and predict the particle size distribution of quartz sandstone produced by high-pressure gas rapid unloading at various infiltration pressures.

## ARTICLE INFO

*Keywords:*
Quartz sandstone
Particle size distribution
Rosin-Rammler function
High-pressure gas
Infiltration pressure

## ABSTRACT

Particle size distribution (PSD) is vital to particles as it determines the quality, safety, and performance of the final product. Rosin-Rammler function (R-R function) is probably the most suitable basic model to characterize the ore powders obtained from comminution. In this paper, we correlate the infiltration pressure with the R-R function to describe the PSD of quartz sandstone produced by high-pressure gas rapid unloading at different infiltration pressures. First, the pulverization experiments of quartz sandstone are conducted in the laboratory. As the infiltration pressure increases from 10 MPa to 25 MPa, producing more fine particles and the mass percentage of −0.5 mm and − 150 μm particles reach 85% and 45%, respectively. Then, based on Dimensional Analysis and assumptions, we assumed that the non-uniformity coefficient and the average particle size in the R-R function are both power functions of infiltration pressure. Finally, the experimental data is used as the learning sample to determine the undetermined parameters in the R-R function using Least Squares. By introducing the infiltration pressure the R-R function can describe and predict the PSD at different infiltration pressures. And the value of the parameters in the R-R function demonstrates that the higher the infiltration pressure, the smaller the average particle size and the more uniform particle distribution. In addition, we also discuss the application of Dimensional Analysis and Least Squares in solving complex problems. We hold that an appropriate basic model is key to obtaining good fitting results. This topic correlates the infiltration pressure with the R-R function to

* Corresponding author.
*E-mail address:* rsyem123@163.com (R. Yang).

https://doi.org/10.1016/j.powtec.2022.117982
Received 16 August 2022; Received in revised form 29 September 2022; Accepted 30 September 2022
Available online 5 October 2022

describe the PSD. On one hand, it reveals the significant influence of infiltration pressure on quartz sandstone pulverization. On the other hand, it also conveys the idea that Dimensional Analysis and Least Squares can indeed conduce to analyze complex problems under a reasonable basic model.

## 1. Introduction

The history of the human application of ore powder can date back to ancient Egypt when people mixed sand into the mud to build pyramids [1]. With the development of society, ore powder has been applied to various fileds supporting the national economy and national security such as medical treatment, construction, national defense, etc. [2]. The multiple-stage crushing together with the ball milling process is the most widely used ore comminution technology [3,4]. Although traditional technology has pretty matured after nearly a hundred years of development, comminution is still an energy-intensive process [4]. An investigation of the energy consumption on mineral comminution showed that it consumes up to 4% of the world-generated electricity, accounting for 50% of overall mining energy consumption [5]. Since the signing of the Paris Agreement in 2015, more than 110 countries have participated in the agreement. Energy conservation and emission reduction are gradually becoming the common goal of all countries in the world [6,7]. However, due to the high energy consumption of ore comminution, the ore processing plants emit countless carbon dioxide every year. On the other hand, with the utilization of a large number of mineral resources over the years, the percentage of lean ore in nonferrous metals, ferrous metals, metallurgy, chemical industry, light industry, and other raw resources is increasing. Correspondingly, the task volume of comminution for liberating valuable minerals is increasing rapidly, which will inevitably lead to more energy consumption and carbon emission. On account of this, it's urgent to develop new technology for ore crushing with low energy consumption and high efficiency.

Many grinding and pretreatment technologies that aim to reduce energy consumption have significantly developed over the last few decades, such as Water jet comminution, Bio-milling, Radiofrequency heating, High-power electromagnetic pulses, and Shock wave pretreatment [8–17]. Among them, the rapid unloading of gas to pulverize ore is an emerging technology in recent years. It applies the equal stress loading on the ore single crystal scale to overcome the interparticle tensile strength to realize the ore pulverization. The comminution mechanisms of several methods are illustrated in Table 1. As we all know, most ores are typical heterogeneous material, as researches show the energy consumed by ore tensile failure is about 1/10 of which by compression failure [18]. As the high efficiency and low energy consumption, the method is probably one of the most promising technologies in the emerging technology for ore pulverization. There has been extensive research about the emerging ore powdering technology [19–22].

PSD is probably the most vital single physical characteristic of particles. It determines the quality, safety, and performance of the final product [23]. Many mathematical models suit to describe the PSD. The most commonly used models are Rosin-Rammler function and Gates-Gaudin-Schuhmann (GGS) [24,25]. Different models apply to specific fields, and research indicates that the R-R function model is most suitable to characterize powders obtained from grinding, milling, and crushing operations [26]. There are two parameters in the R-R function, representing the average size and degree of inhomogeneity of the ore particles, respectively. As long as these two parameters are determined, the R-R function can describe the cumulative PSD pretty well. However, the two parameters are too simple to directly reflect the influence of comminution condition on the PSD. In this paper, we correlate the infiltration pressure with the R-R function to describe the PSD of quartz sandstone produced by gas rapid unloading at different infiltration pressure. The quartz sandstone laboratory pulverization experiments

**Table 1**
The grinding mechanism of different comminution methods.

| Destruction Mechanism | b. Split | a. Crush | c. Bend | d. Grinding | e. Impact |
|---|---|---|---|---|---|
| Jaw crusher | √ | √ | √ | × | × |
| Cone crusher | × | √ | √ | × | × |
| Ball mill | × | × | √ | √ | √ |

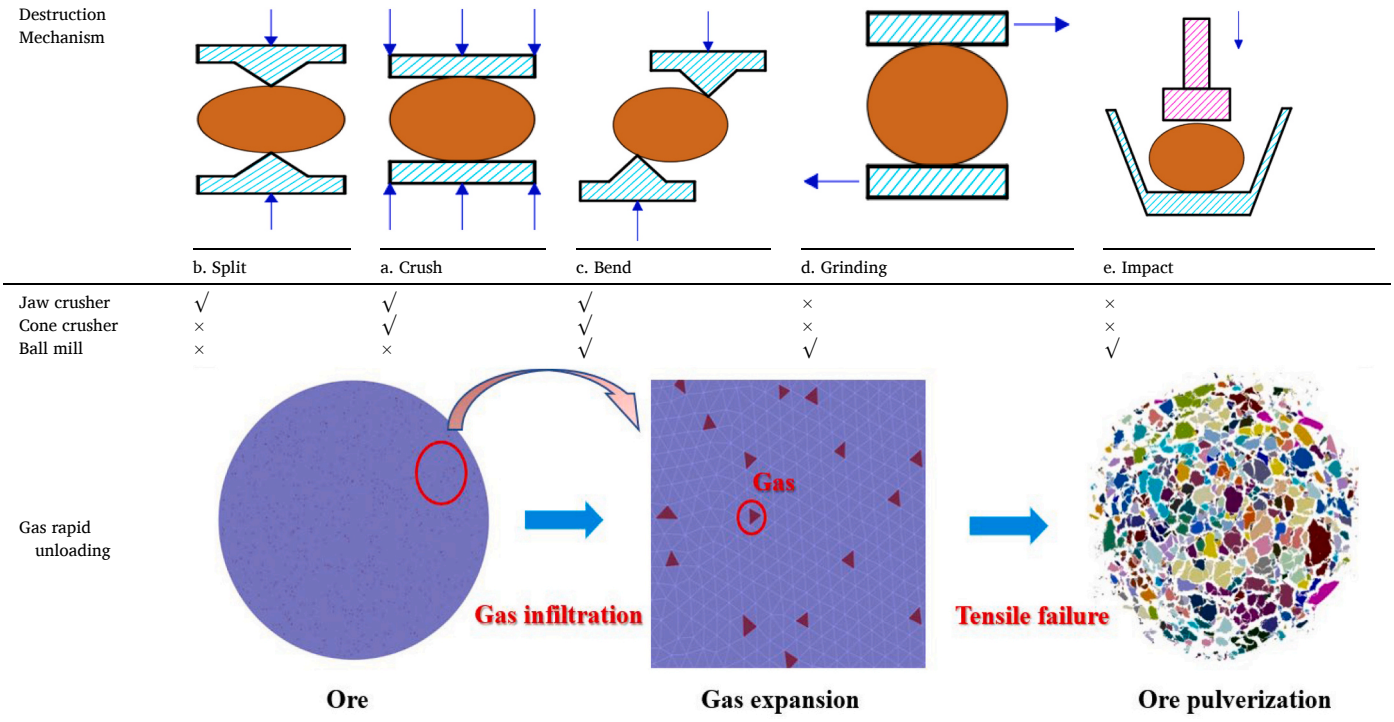

were conducted at various infiltration pressure at first. Then, correlating the infiltration pressure with the R-R function based on the assumption that the non-uniformity coefficient and the average particle size are both power functions of infiltration pressure. Finally, the R-R function can describe and predict the PSD of quartz sandstone obtained at different infiltration pressure.

## 2. Experimental methodology

### 2.1. Materials and method

Quartz sandstone, also known as feldspar sandstone, is mainly composed of quartz and feldspar. It has wide application in the foundry industry and refractory production as good refractoriness. The main chemical components of quartz sandstone are silica ($SiO_2$) and alumina ($Al_2O_3$), which is used to produce glass fibers in recent years. The chemical composition of quartz sandstone is illustrated in Table 2.

We conducted high-pressure gas high-speed unloading and powdering quartz sandstone experiments in the laboratory. The pulverization experiment apparatus consists of the high-pressure infiltration chamber and the high-pressure propulsion chamber. In the front of the infiltration chamber, there is a rupture disk, which separates the infiltration chamber from the atmosphere. The high-pressure gas propulsion ensures the ore leaves the outlet at high speed. Put the quartz sandstone into the high-pressure infiltration chamber via the outlet before the rupture disk installation. The schematic diagram of the experimental apparatus is illustrated in Fig. 1.

### 2.2. Experiment implementation

We designed four group pulverization experiments of quartz sandstone at the infiltration pressures of 10 MPa, 15 MPa, 20 MPa, and 25 MPa, respectively. And the corresponding propulsion pressures are 15 MPa, 20 MPa, 25 MPa, and 30 MPa. The purpose of propulsion pressure higher than infiltration pressure is to keep the quartz sandstone spout out from the high-pressure infiltration chamber at high speed. It ensures the high-pressure gradient inside and outside the quartz sandstone, which is conducive to its pulverization. The mass of quartz sandstone for each experiment is approximately 1.5 kg. The width of the quartz sandstone is about 10 cm because the inner diameter of the infiltration chamber is 10 cm. All the experimental parameters are presented in Table 3.

The steps for quartz sandstone pulverization experiments are as follows. Firstly, Put the quartz sandstone into the high-pressure infiltration chamber via the outlet. Second, the rupture disc is installed in the high-pressure infiltration chamber. Third, filling the high-pressure air into the high-pressure infiltration chamber. After air filling, the equipment was put into the collection chamber and the infiltration chamber and connected to the propulsion chamber. And then high-pressure gas was injected into the propulsion chamber. Finally, detonate the explosives to burst the rupture disc and ore spouts from the high-pressure infiltration chamber together with high-pressure air into the collection chamber.

The gas pressure outside the quartz sandstone dropped much more quickly than which inside the internal pores, forming a high-pressure gradient inside and outside the ore in a short time. The ore will expand from the inside out and eventually pulverize once the pressure gradient overcomes the interparticle tensile strength. After experiment, the quartz sandstone powder was taken out of the collection chamber and screened. A detailed procedure is introduced in the papers [20,22]. The experiment apparatus is illustrated in Fig. 2.

It is worth noting that the gas used to pulverize the ore in the previous study was liquid $CO_2$, whereas in this case, it was high-pressure air. On the one hand, air is an experimental medium that is easier to obtain in the laboratory. On the other hand, it may be necessary to use sodium hydroxide (NaOH) to beneficiate the quartz sandstone after grinding. Therefore, carbon dioxide should be avoided as far as possible in the quartz sandstone pretreatment process to exclude it reacts with sodium hydroxide (NaOH). The quartz sandstone before and after the pulverization experiment is illustrated in Fig. 3.

### 2.3. Correlation analysis of the infiltration pressure and PSD

After the experiment, the quartz sandstone with an average size of 10 cm was pulverized into micro-sized particles. Powder properties are affected by particle shape, particle size, and size distribution [27]. The PSD of the quartz sandstone powder under different experimental conditions are illustrated in Fig. 4.

Overall, the infiltration pressure has a significant influence on quartz sandstone pulverization. Raising infiltration pressure mainly affects the distribution of −0.5 mm fine particles. At the four infiltration pressures, the mass percentage of −45 μm particles is 4%, 4%, 4%, and 6%, respectively. It means the mass percentage of this part increases slightly with raising infiltration pressure. Changing the infiltration pressure significantly affects the particle distribution between 80 μm and 150 μm. As the infiltration pressure increases from 10 MPa to 25 MPa, the percentage of particle size between 80 μm and 150 μm boosts from 9% to 16%. However, increasing infiltration pressure reduces the mass percentage of particle size between 150 μm and 500 μm. As the infiltration pressure increases from 10 MPa to 25 MPa, the mass percentage of particle size between 150 μm and 0.5 mm decreases from 56% to 39%. For the coarse particle of +0.5 mm, its mass percentage doesn't change regularly with increasing infiltration pressure.

## 3. Describe the PSD by the R-R function

### 3.1. Rosin-Rammler function

The most common mathematical models utilized to describe the experimental PSD of curves are the R-R function and GGS [26]. Among them, the R-R function is probably the more suitable to characterize the powder obtained from ore pulverization. The general expression of the R-R function is illustrated in Eq. 1.

$$F(x) = 1 - exp\left[-\left(\frac{x}{X_0}\right)^n\right] \tag{1}$$

where $x$ is the particle size (mm), $X_0$ is the particle size with a cumulative rate under sieve of 63.1%, representing the average particle size, $n$ is the non-uniformity coefficient representing the degree of non-uniformity of the particle distribution.

As long as the parameters $X_0$ and $n$ are certain, the R-R function is uniquely determined. The R-R function is too simple to directly reflect the influence of the change of comminution condition on the PSD. In this section, we correlates the parameters $X_0$ and $n$ with the infiltration to describe the PSD obtained at different infiltration pressures.

### 3.2. Simplification and assumptions

High-pressure air destroys quartz sandstone across scales to micron-

**Table 2**
The chemical components of quartz sandstone.

| Composenet | $SiO_2$ | $Al_2O_3$ | CaO | MgO | $Fe_2O_3$ | $K_2O$ | $Na_2O$ | $TiO_2$ | $SO_3$ | LOI |
|---|---|---|---|---|---|---|---|---|---|---|
| Mass ratio (%) | 82.33 | 11.92 | 0.04 | 0.11 | 0.53 | 0.57 | 0.02 | 0.44 | 0.05 | 3.99 |

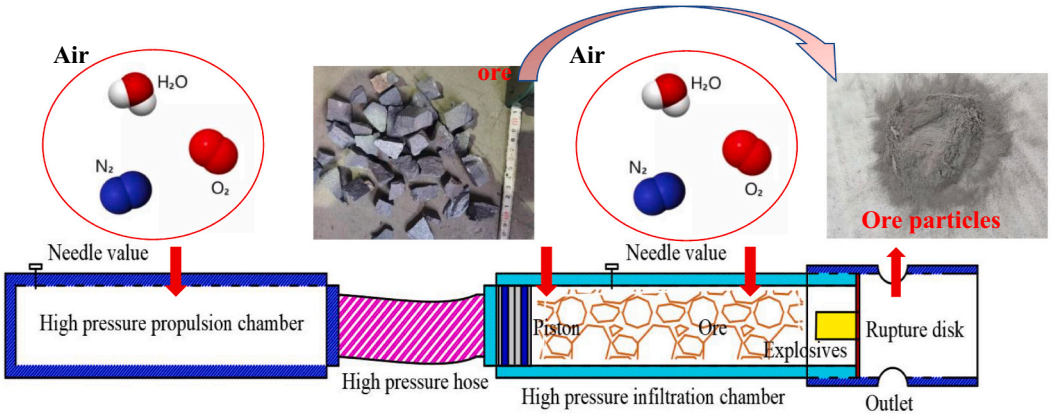


**Fig. 1.** Schematic diagram of the experiment apparatus.

**Table 3**
Experimental parameters.

| Parameters | Group 1 | Group 2 | Group 3 | Group 4 |
|---|---|---|---|---|
| Weight (kg) | 1.5 | 1.5 | 1.5 | 1.5 |
| Quartz sandstone size (cm) | 10–15 | 10–15 | 10–15 | 10–15 |
| Infiltration gas pressure (MPa) | 10 | 15 | 20 | 25 |
| Propulsion gas pressure (MPa) | 15 | 20 | 25 | 30 |
| The thickness of the rupture disk (mm) | 5 | 5 | 6 | 6 |

sized particles in milliseconds during rapid unloading. We analyzed the experimental process by Dimensional Analysis to simplify the problem. We chose the particle diameter of quartz sandstone, the density of quartz sandstone, and the interparticle tensile strength of quartz sandstone as repeat variables. It is easy to see that density has mass (M) appearing uniquely in it, interparticle tensile strength has time (T) appearing in it, and the diameter has the length (L). The three variables can't form a dimensionless group as a result. All other variables that may affect the PSD were represented as dimensionless groups by the repeated variables. The result of dimension analysis is illustrated in Table 4.

The parameters $X_0$ and $n$ are written as functions of dimensionless groups respectively. The functions are illustrated in Eq. 2.


**Fig. 2.** Experiment apparatus for ore pulverization.


**Fig. 3.** Quartz sandstone before and after the experiment. (a) The quartz sandstone (b) The quartz sandstone powder.

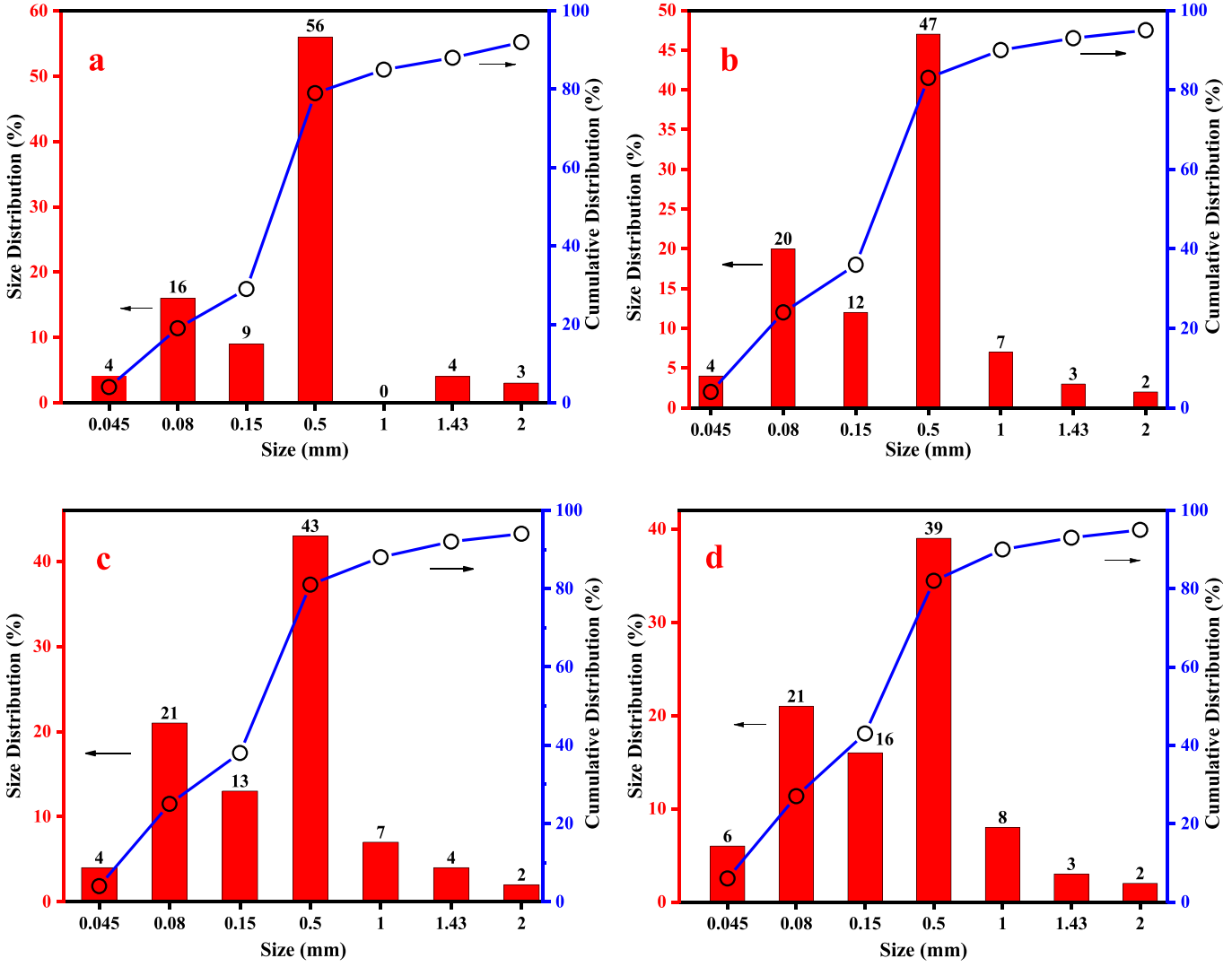


**Fig. 4.** Particle size distribution of the quartz sandstone powder at different infiltration pressure experimental. (a) 10 MPa (b) 15 MPa (c) 20 MPa (d) 25 MPa.

$$\begin{cases} \dfrac{X_0}{L_1} = f\left(\phi, \dfrac{r_1}{L_1}, \dfrac{D_1}{L_1}, \dfrac{K}{L_1^2}, \dfrac{E}{\sigma_t}, \dfrac{G_f}{\sigma_t L_1}, \dfrac{P_{in}}{\sigma_t}, \dfrac{\mu}{(\sigma_t)^{\frac{1}{2}}(\rho_1)^{\frac{1}{2}}L_1}, \dfrac{L_2}{L_1}, \dfrac{L_3}{L_1}\right) \\ n = g\left(\phi, \dfrac{r_1}{L_1}, \dfrac{D_1}{L_1}, \dfrac{K}{L_1^2}, \dfrac{E}{\sigma_t}, \dfrac{G_f}{\sigma_t L_1}, \dfrac{P_{in}}{\sigma_t}, \dfrac{\mu}{(\sigma_t)^{\frac{1}{2}}(\rho_1)^{\frac{1}{2}}L_1}, \dfrac{L_2}{L_1}, \dfrac{L_3}{L_1}\right) \end{cases} \tag{2}$$

In Eq. (2), the first four dimensionless groups represent quartz sandstone properties, the middle two character the gas properties, and the last two represent experimental equipment parameters. In the laboratory experiments, nothing changed but the infiltration pressure. As a result, it is the middle two dimensionless groups related to high-pressure gas that mainly affects the non-uniformity coefficient $n$ and the average particle size $X_0$. On the other hand, the temperature controls the viscosity of the fluid, and pressure change has little effect on the dynamic viscosity of the air. When the temperature is constant, the dynamic viscosity of air is $2.05 \times 10^{-5}$ Pa·s, $2.21 \times 10^{-5}$ Pa·s, $2.4 \times 10^{-5}$ Pa·s, and $2.6 \times 10^{-5}$ Pa·s at the pressure of 10 MPa, 15 MPa, 20 MPa, and 25 MPa, respectively. It suggests that the dynamic viscosity of air changes very little with pressure. We also disregarded the influence of the dynamic viscosity of air in consequence. The air density and dynamic viscosity at different pressures are shown in Fig. 5.

According to the above analysis, we took the non-uniformity coefficient and the average particle size as functions of the dimensionless group containing infiltration pressure, respectively. To further simplify the problem, we assumed that these two parameters are the power function of the dimensionless groups. The formula derivation process is illustrated in Eq. (3). The $\frac{L_1}{\sigma_t^{\partial}}$ and $\frac{1}{\sigma_t^{\beta}}$ were denoted as $C_1$ (m/MPa$^{\alpha}$) and $C_2$ (1/MPa$^{\beta}$).

$$\begin{cases} \dfrac{X_0}{L_1} = f\left(\dfrac{P_{in}}{\sigma_t}\right) \\ n = g\left(\dfrac{P_{in}}{\sigma_t}\right) \end{cases} \Rightarrow \begin{cases} X_0 = L_1\left(\dfrac{P_{in}}{\sigma_t}\right)^{\partial} = \dfrac{L_1}{\sigma_t^{\partial}}(P_{in})^{\partial} \\ n = \left(\dfrac{P_{in}}{\sigma_t}\right)^{\beta} = \dfrac{1}{\sigma_t^{\beta}}(P_{in})^{\beta} \end{cases} \Rightarrow \begin{cases} X_0 = C_1(P_{in})^{\partial} \\ n = C_2(P_{in})^{\beta} \end{cases} \tag{3}$$

As shown in Eq. (3), the average particle size is affected by the interaction between the infiltration pressure and the interparticle tensile strength and the inherent particle size of the ore as well. The non-uniformity coefficient is only a result of the interaction between the infiltration pressure and the interparticle tensile strength. The the high-pressure gas applies equal stress loading on the ore single crystal scale to overcome the interparticle tensile strength. The PSD at a certain infiltration pressure is affected by the interparticle tensile strength, infiltration pressure, and the inherent size of the ore particles. Although we only varied the infiltration pressure in our experiments, the effect of ore properties on PSD is ubiquitous. The Dimensional Analysis introduces the interparticle tensile strength, and the ore particle size, into the analysis process by forming dimensionless groups. It is where the unique appeal of Dimensional Analysis comes in, providing a way to analyze the

**Table 4**
Dimension analysis about quartz sandstone pulverization.

| Variable | Symbol | Dimension | Dimensionless Group |
|---|---|---|---|
| Size of quartz sandstone particles | $L_1$ | $L$ | Repeat variable |
| Density of quartz sandstone | $\rho_1$ | $\frac{M}{L^3}$ | Repeat variable |
| Interparticle tensile strength | $\sigma_t$ | $\frac{M}{T^2L}$ | Repeat variable |
| Porosity of quartz sandstone | $\phi$ | 1 | $\phi$ |
| Pore size of quartz sandstone | $r_1$ | $L$ | $\frac{r_1}{L_1}$ |
| Size of quartz sandstone | $D_1$ | $L$ | $\frac{D_1}{L_1}$ |
| Penetration | $K$ | $L^2$ | $\frac{K}{L_1^2}$ |
| Elastic Modulus of quartz sandstone | $E$ | $\frac{M}{T^2L}$ | $\frac{E}{\sigma_t}$ |
| Fracture energy of quartz sandstone | $G_f$ | $\frac{M}{T^2}$ | $\frac{G_f}{\sigma_t \cdot L_1}$ |
| Gas Pressure | $P$ | $\frac{M}{T^2L}$ | $\frac{P_{in}}{\sigma_t}$ |
| Gas dynamic viscosity | $\mu$ | $\frac{M}{LT}$ | $\frac{\mu}{(\sigma_t)^{\frac{1}{2}} \cdot (\rho_1)^{\frac{1}{2}} \cdot L_1}$ |
| Diameter of the infiltration chamber | $L_2$ | $L$ | $\frac{L_2}{L_1}$ |
| Length of the infiltration chamber | $L_3$ | $L$ | $\frac{L_3}{L_1}$ |
| Index of particle uniformity | $n$ | 1 | $n$ |
| Diameter for 63.2% particles pass | $X_0$ | $L$ | $\frac{X_0}{L_1}$ |

causal relationships between physical phenomena and physical quantities. Substituting Eq. (3) into Eq. (1) yields Eq. (4). As long as the parameters $C_1$, $C_2$, $\alpha$ and $\beta$ are determined, the R-R function can be determined. Besides, the parameters are closely related to the interparticle tensile strength and the ore particle size. We can compare the interparticle tensile strength and particle size of different ores by comparing the values of these parameters in the subsequent research.

$$F(x) = 1 - exp\left[ -\left( \frac{x}{C_1 (P_{in})^{\partial}} \right)^{C_2 (P_{in})^{\beta}} \right] \tag{4}$$

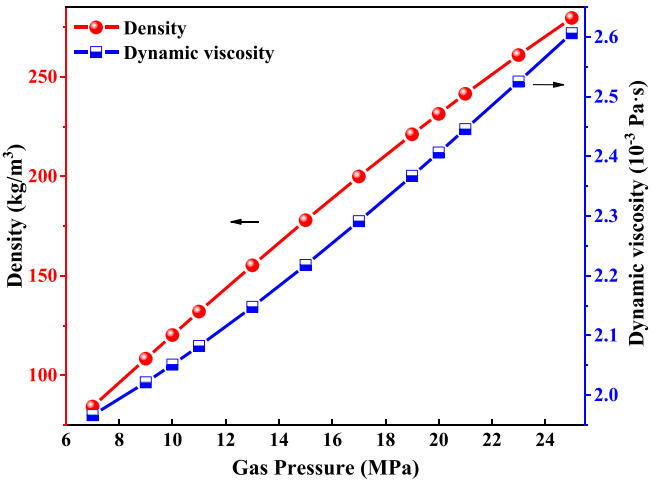


**Fig. 5.** Air density and dynamic viscosity at different pressures.

where $F(x)$ is the distribution function, and $x$ is the particle size (mm), $P_{in}$ is the infiltration pressure (MPa), $C_1$, $C_2$,$\alpha$ and $\beta$ are undetermined parameters.

### 3.3. Parameters determination

The experimental data (10 MPa, 15 MPa, and 25 MPa) were taken as learning samples to determine the undetermined parameters in Eq. (4) by Least Squares. Least Squares is a mathematical tool for data processing. It is used in a wide range of disciplines such as error estimation, uncertainty system identification, and forecasting since first proposed by Gauss [28]. The theoretical function is illustrated in Eq. (5). Bring Eq. (4) and experimental data into Eq. (5) to obtain the residual function. The residual function is illustrated in Eq. (5).

$$\delta = \sum_{i=1}^{m} [F(x_i, C_1, C_2, \alpha, \beta) - y_i]^2 \tag{5}$$

where the $m$is the number of samples data, $(x_i, y_i)$ is the samples data and the $C_1$, $C_2$, $\alpha$ and $\beta$ are the undertermined parameters, respectively.

$$\delta = \left\{ \begin{array}{l} \left(1 - exp\left(-\frac{0.045}{C_1(10)^{\alpha}}\right)^{C_2(10)^{\beta}} - 0.04\right)^2 + \left(1 - exp\left(-\frac{0.08}{C_1(10)^{\alpha}}\right)^{C_2(10)^{\beta}} - 0.02\right)^2 + \left(1 - exp\left(-\frac{0.15}{C_1(10)^{\alpha}}\right)^{C_2(10)^{\beta}} - 0.29\right)^2 \\ + \left(1 - exp\left(-\frac{0.5}{C_1(10)^{\alpha}}\right)^{C_2(10)^{\beta}} - 0.85\right)^2 + \left(1 - exp\left(-\frac{1}{C_1(10)^{\alpha}}\right)^{C_2(10)^{\beta}} - 0.85\right)^2 + \left(1 - exp\left(-\frac{1.43}{C_1(10)^{\alpha}}\right)^{C_2(10)^{\beta}} - 0.89\right)^2 \\ + \left(1 - exp\left(-\frac{2}{C_1(10)^{\alpha}}\right)^{C_2(10)^{\beta}} - 0.92\right)^2 + \left(1 - exp\left(-\frac{0.045}{C_1(15)^{\alpha}}\right)^{C_2(15)^{\beta}} - 0.04\right)^2 + \left(1 - exp\left(-\frac{0.08}{C_1(15)^{\alpha}}\right)^{C_2(15)^{\beta}} - 0.24\right)^2 \\ + \left(1 - exp\left(-\frac{0.15}{C_1(15)^{\alpha}}\right)^{C_2(15)^{\beta}} - 0.36\right)^2 + \left(1 - exp\left(-\frac{0.5}{C_1(15)^{\alpha}}\right)^{C_2(15)^{\beta}} - 0.83\right)^2 + \left(1 - exp\left(-\frac{1}{C_1(15)^{\alpha}}\right)^{C_2(15)^{\beta}} - 0.9\right)^2 \\ + \left(1 - exp\left(-\frac{1.43}{C_1(15)^{\alpha}}\right)^{C_2(15)^{\beta}} - 0.93\right)^2 + \left(1 - exp\left(-\frac{2}{C_1(15)^{\alpha}}\right)^{C_2(15)^{\beta}} - 0.95\right)^2 + \left(1 - exp\left(-\frac{0.045}{C_1(25)^{\alpha}}\right)^{C_2(25)^{\beta}} - 0.06\right)^2 \\ + \left(1 - exp\left(-\frac{0.08}{C_1(25)^{\alpha}}\right)^{C_2(25)^{\beta}} - 0.27\right)^2 + \left(1 - exp\left(-\frac{0.15}{C_1(25)^{\alpha}}\right)^{C_2(25)^{\beta}} - 0.43\right)^2 + \left(1 - exp\left(-\frac{0.5}{C_1(25)^{\alpha}}\right)^{C_2(25)^{\beta}} - 0.82\right)^2 \\ + \left(1 - exp\left(-\frac{1}{C_1(25)^{\alpha}}\right)^{C_2(25)^{\beta}} - 0.9\right)^2 + \left(1 - exp\left(-\frac{1.43}{C_1(25)^{\alpha}}\right)^{C_2(25)^{\beta}} - 0.93\right)^2 + \left(1 - exp\left(-\frac{2}{C_1(25)^{\alpha}}\right)^{C_2(25)^{\beta}} - 0.95\right)^2 \end{array} \right\} \tag{6}$$

As shown in Eq. (6), the PSD obtained by experiments at infiltration pressure of 10 MPa, 15 MPa, and 25 MPa were taken as training samples. Usually, the next step is to take the partial derivative of the residual function to obtain the system of equations. And then, solve the system of equations to determine the undetermined parameters. The system of equations is illustrated in Eq. (7).

$$\begin{cases} \dfrac{\partial\delta}{\partial C_1}=0, \dfrac{\partial\delta}{\partial\alpha}=0 \\ \dfrac{\partial\delta}{\partial C_2}=0, \dfrac{\partial\delta}{\partial\beta}=0 \end{cases} \tag{7}$$

However, Eq. (7) is too complicated to solve. Some mathematical software can quickly solve complex equations. Mathematic, a powerful mathematical software, was used in this paper to solve for the undetermined parameters that minimize the residual function. The code for solving the undetermined parameters in Mathematic is shown in Eq. (8).

$$FindMinimum[\delta,\{C_1,a_0\},\{C_2,b_0\},\{\partial,c_0\},\{\beta,d_0\}] \tag{8}$$

Where $\delta$ is the residual function, $C_1$, $C_2$, $\alpha$ and $\beta$ are the undetermined parameters, $a_0$, $b_0$, $c_0$,$d_0$ are the starting values of the undetermined parameters, respectively.

It was calculated that the residual function $\delta$=0.0742 and the parameters $C_1$=0.4976, $C_2$=1.6970, $\alpha$= − 0.1499 and $\beta$= − 0.1833. The parameters were substituted into Eq. (5). The R-R function correlated with the infiltration pressure is illustrated in Eq. (9).

$$F(x)=1-exp\left[-\left(\frac{x}{0.467(P_{in})^{-0.119}}\right)^{1.715(P_{in})^{-0.192}}\right] \tag{9}$$

### 3.4. Theoretical results validation

In addition, it is worth mentioning that the solution obtained by math software may be local rather than globally optimal. Its rationality needs verifying by comparing it with experimental data, which is illustrated in Fig. 6. The PSD obtained at the infiltration pressure is 20 MPa was token as the test sample to judge the accuracy of the R-R function for PSD prediction.

By correlating with the infiltration pressure, the R-R function can generally well describe the PSD obtained at different infiltration pressure (Fig. 6a-c). In the range of 80 μm–150 μm, where the quartz sandstone particles are most concentrated, the R-R function has a good fit quality to the experimental data. It demonstrates that the undetermined parameters determined with mathematical software are reasonable. The value of undetermined parameters $C_1$=0.4976 and $\alpha$= − 0.1499, respectively. It indicates that the average particle size of the ore

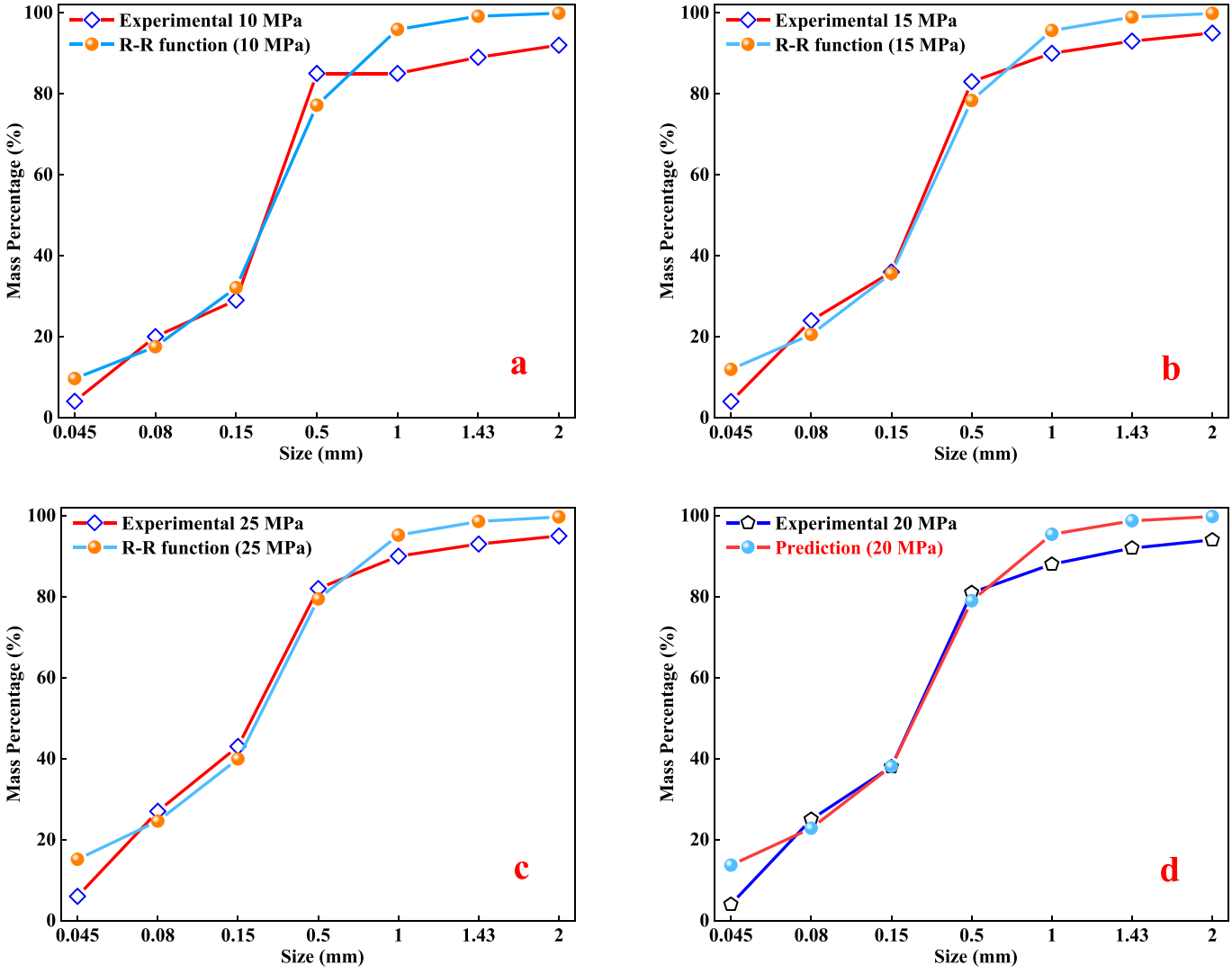


**Fig. 6.** Comparison of PSD obtained by R-R function and experiment. (a) 10 MPa (b) 15 MPa (c) 25 MPa, (d) 20 MPa.

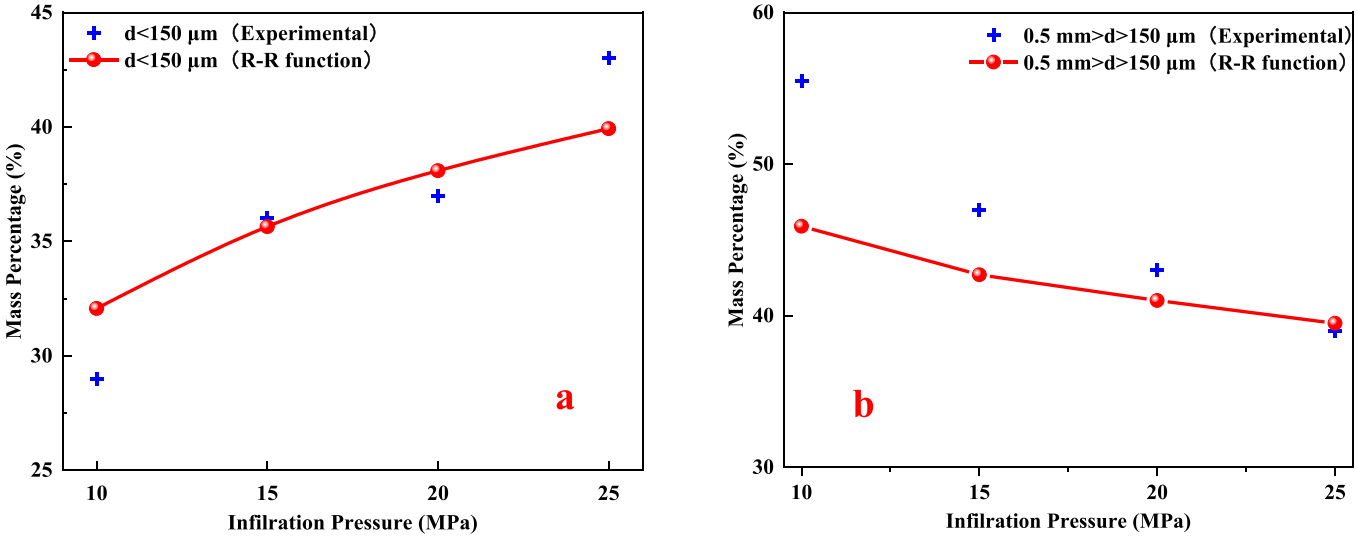


**Fig. 7.** The R-R function fits −0.5 mm quartz sandstone PSD changing with infiltration pressure (a) -150 μm (b) 150 μm-0.5 mm.

particles decreases as the pressure increases. Meanwhile $C_2$=1.6970 and $\beta$= − 0.1833, which suggest a more uniform particle distribution with boosting pressure. The R-R function fits well with the test sample (Fig. 6d). The R-R function can predict the PSD obtained at different infiltration pressures without conducting experiments. By correlating with the infiltration pressure, the R-R function provides convenience in analyzing the effect of infiltration pressure on PSD.

While Fig. 6 illustrates that by correlating to infiltration pressure, the R-R function can describe the cumulative PSD at different infiltration pressures, failing to reflect its fit quality in describing PSD changing with infiltration pressure. Increasing infiltration pressure mainly affects the distribution of −0.5 mm fine particles. For the coarse particle of +0.5 mm, its mass percentage doesn't change regularly with raising infiltration pressure. The R-R function has good fit quality on the −150 μm particles mass percentage changing infiltration pressure well, with the maximum error of about 3% appearing at the infiltration pressure is 25 MPa (Fig. 7a). The R-R function also shows good fitness to coarse particles of 150 μm-0.5 mm. At the infiltration pressure is 10 MPa, the R-R function has about a 10% error with the experimental data (Fig. 7b). The experiment at infiltration pressure is 10 MPa produces excessive 150 μm-0.5 mm particles and almost no 0.5 mm–1 mm particles produced. While it did not fundamentally affect the whole fit results and quality, the error between the fitted results and these experiment data is obvious.

## 4. Result and discussion

### 4.1. Result

The infiltration pressure is introduced into the R-R function to analyze the PSD of quartz sandstone produced by high-pressure gas rapid unloading at different infiltration pressures. The laboratory experiments were carried out at various infiltration pressures first. And then, the R-R function is correlated with infiltration pressure using Dimension Analysis. Finally, the undetermined parameters in the R-R function are determined according to the experimental data by Least Squares. After introducing the infiltration pressure, the R-R function can directly reflect the influence of infiltration pressure on the average size and degree of inhomogeneity of ore particles and predict the PSD obtained at different infiltration pressures.

The PSD obtained in the laboratory experiments is listed in Fig. 4. It depicts the influence of infiltration pressure on the PSD of quartz sandstone. At the infiltration pressure of 25 MPa, the percentage of particles between 80 μm–50 μm is 16%, which is a 9% improvement over 10 MPa. For coarse particles, the mass percentage between 150 μm-0.5 mm is 39%, which is 17% lower than at 10 MPa. It indicates that raising the infiltration pressure produces more coarse and less fine particles. However, there is no significant effect on the mass percentage of +0.5 mm particles. Meanwhile, the experimental results also show the high-pressure gas rapid unloading technique for pulverizing ore applicate for quartz sandstone. On the other hand, It reveals the influence of infiltration pressure on the pulverization effect of quartz sandstone.

The R-R function correlated with the infiltration pressure is illustrated in Eq. 9. The parameters in R-R function $C_1$=0.4976 and $\alpha$= − 0.1499, respectively. It indicates that the average particle size of the ore particles decreases as the pressure increases. Meanwhile $C_2$=1.6970 and $\beta$= − 0.1833, demonstrate a more uniform particle distribution with raising infiltration pressure. The load applied on the ore single crystal scale boosts as the rise of infiltration pressure. It undoubtedly results in ore more pulverized with smaller average particle size. The effect of the random structure of the ore on the ore pulverization will diminish as the load increases. As a result, the PSD of the powder produced by the high-speed unloading of the gas under high infiltration pressure is more uniform. We tentatively conclude that the parameters compounds the underlying objective law. A comparison between the experimentally obtained PSD and the R-R function is shown in Figs. 6–7. It further suggests that the R-R function associated with the infiltration pressure is reasonable and can describe the PSD of quartz sandstone obtained at different infiltration pressures.

It is chosen a suitable basic model and introduced a reasonable variable that we obtained good fit results. On the one hand, the R-R function, as a basic model, has been shown by many studies to be particularly suitable for describing the particle distribution of powders produced by comminution. It could not have been chosen more appropriately as the basic mathematical model for describing the PSD of quartz sandstone. On the other hand, there was little (if any negligible) variation in this study other than the infiltration pressure. It is reasonable to treat the mean particle size and the non-uniformity coefficient as a function of the dimensionless group containing infiltration pressure.

### 4.2. Discussion about the error between the theoretical results and experimental data

It also can be seen in Fig. 6 that when the particle diameter is smaller than 80 μm and larger than 0.5 mm, the PSD calculated by the R-R function has significant errors with the experimental data. These errors are mainly due to the assumed functional form being unreasonable and

the inaccuracy of the experimental data. Admittedly, the assumption that the mean particle size and the inhomogeneity index in the R-R function are power functions of the infiltration pressure is debatable. According to the R-R, the mass percentage of particles with a particle size less than 45 μm increases with increasing infiltration pressure. However, the experimental results show that the increasing infiltration pressure has almost no effect on the mass percentage of particles smaller than 45 μm. Likewise, the percentage of particles larger than 0.5 mm varies very little with infiltration pressure. However, the calculation of the R-R function shows that it decreases with increasing infiltration pressure. Perhaps a polynomial is a more appropriate functional form as Taylor's formula has been widely utilized to fit complex functions [29,30]. However, it's no doubt that the polynomials will introduce more undetermined parameters into the R-R function. How to determine these parameters will be the focus of subsequent research.

The experiment at infiltration pressure is 10 MPa produces excessive 150 μm-0.5 mm particles and almost no 0.5 mm–1 mm particles produced, which may lead to a significant error between the fitted results and experiment data (Fig. 6a and Fig. 7b). Therefore, We attempted certain the undetermined parameters in the R-R function more reasonably by using a learning sample without the two data. The fit gives a residual function $\delta$=0.0578 and the undetermined parameters $C_1$=0.3242, $\alpha$= − 0.099, $C_2$=3.0789, and $\beta$= − 0.191699, respectively. It suggests that the average size and inhomogeneity of the quartz sandstone particles became smaller with increasing infiltration pressure, which is consistent with previous findings. However, the residual function decreases by 20% relative to the previous value of 0.07. Thus, although the individually unreasonable data did not fundamentally affect the conclusions, it increased the error between the fitted results and the experimental data as a whole.

### 4.3. Discussion about the application of dimensional analysis and least squares

Dimensional Analysis and Least Squares, two old but widely used methods, can indeed help solve some complex problems. Dimensional Analysis helps to reveal relationships between physical phenomena and physical quantities. Selecting suitable repeated variables is the key and arduous point of Dimensional Analysis. As shown in this paper, it is taking particle size and the inter-particle tensile strength of Quartz Sandstone as the repeated variables that obtain the appropriate dimensionless group and follow-up results. The Least Squares contribute to determining the theoretical model that has the least error with the experimental data. A suitable base model is key to utilizing the method to study complex problems. However, it is difficult to generalize a concise and appropriate mathematical model for complex questions. It requires in-depth research and a long-term accumulation of scholars in related fields. Even the currently popular neural network approach uses complex neural network structures as an abstract model for complex non-linear questions, rather than giving explicit functional forms. The result is that even if obtaining a good fit result, the mapping relationship between input and output is not clear.

An appropriate basic model allows further analyze the specific functional relationship between input and output using Dimensional Analysis and Least Squares. In addition to infiltration pressure, we can also use the methods to analyze the effect of process operating conditions such as ore size on PSD and even problems in other fields. For example, the strain rates have a significant influence on the stress-strain relationship of the material. When the material is in the elastic stage, its stress-strain relationship satisfies the generalized Hooke's law. The modulus of elasticity of wood increases substantially with the loading rate [31]. According to the viewpoint of this paper, regarding the generalized Hooke's law as the basic model. Taking the modulus of elasticity of wood as a function of loading rate to modify the generalized Hooke's law. Then, obtain the wood stress-strain curves at different strain rates in the laboratory. Finally, using the experimental data as a learning sample, the expression of the generalized Hooke's law correlates with the strain rates determined by the least-squares method. In this way, Hooke's law can describe the stress-strain relationship of wood at different strain rates.

### 4.4. Discussion about the following work

In follow-up researchers, we will focus on investigating more suitable functional forms to describe the effect of comminution parameters on the average and non-uniformity of the ore particles. Further experiments will also conduct to optimize the current R-R function and verify its applicability in describing the PSD of other ores after pulverization. If possible, we will also apply Dimensional Analysis and Least Squares to problems in other areas. Another unsolved question is the ore pulverization process by the high-pressure gas rapid unloading. Direct observation of the ore pulverization process is arduous and dangerous as its extreme speed and high gas pressure. High-speed cameras and some optical instruments may help solve this problem.

## 5. Conclusion

The paper aims to correlate the infiltration pressure with the R-R function to describe the PSD of quartz sandstone produced by high-pressure gas rapid unloading at different infiltration pressure. As infiltration pressure increases from 10 MPa to 25 MPa, producing more fine particles and the mass percentage of −0.5 mm and − 150 μm particles reach 85% and 45%, respectively. Given can't directly reflect the effect of infiltration pressure on PSD, introducing infiltration pressure into the R-R function as a variable using Dimensional Analysis and Least Squares.

The R-R function correlated with infiltration pressure provides a good description and prediction of the quartz sandstone PSD obtained at different infiltration pressures. The parameters of the R-R function suggest that the quartz sandstone particle's average particle size and inhomogeneity decrease as the infiltration pressure increases. Meanwhile, the paper also conveys the idea that Dimensional Analysis and Least Squares conduce us to solve some complex problems under a reasonable basic model. An appropriate basic model is a prerequisite for obtaining good fitting results. In addition, the accuracy of the experimental data plays an important role. For the Least Squares, the experimental data is used as a learning sample to find the residual function. The incorrect experimental data affects the accuracy of the fit results.

By introducing the infiltration pressure, the R-R function allows a better analysis of the effect of infiltration pressure on ore pulverization. It also provides a way to predict the PSD obtained at different infiltration pressures without experimentation. The idea of correlating the R-R function with ore process condition using Dimensional Analysis and Least Squares is also suited to analyze the effect of comminution parameters other than infiltration pressure on PSD. The approach even applies to other areas outside the field of ore pulverization.

## Data availability

Data will be made available on request.

## CRediT authorship contribution statement

**Genghao Zhang:** Conceptualization, Investigation, Data curation, Writing – original draft, Writing – review & editing, Methodology, Formal analysis. **Yongbo Fan:** Methodology, Formal analysis, Writing – review & editing. **Renshu Yang:** Methodology, Supervision, Resources, Formal analysis, Funding acquisition. **Shihai Li:** Resources, Methodology, Writing – review & editing, Formal analysis.

## Declaration of Competing Interest

The authors declare that they have no known competing financial

interests or personal relationships that could have appeared to influence the work reported in this paper.

## Data availability

Data will be made available on request.

## Acknowledgements

The authors wish to thank Luo H, Wang QL, and Liu HQ for their advice on experimental design. The authors also gratefully acknowledge the financial support from the National Natural Science Foundation of China. [No. 51934001].

## References

[1] O. Molerus, History of Civilisation in the Western Hemisphere from the Point of View of Particulate Technology, History, 1993.
[2] D.N. Oleg, Powders for Additive Manufacturing Processing, Elsevier, Netherlands, 2019, pp. 373–399.
[3] D.N. Oleg, Mechanical Crushing and Grinding, Elsevier, Netherlands, 2019, pp. 65–90.
[4] P. Parisa, R. Jan Mehdi, Quantitative analysis of ore texture breakage characteristics affected by loading mechanism: fragmentation and mineral liberation, Miner. Eng. 182 (2022), 107561.
[5] J. Jack, S. Alex, Energy consumption in mining comminution, Proc. CIRP 48 (2016) 140–145.
[6] P. Agreement, Paris agreement, Report of the Conference of the Parties to the United Nations Framework Convention on Climate Change (21st Session, 2015: Paris). Retrived December, HeinOnline, 2015, p. 2017.
[7] M.-T. Huang, P.-M. Zhai, Achieving Paris agreement temperature goals requires carbon neutrality by middle century with far-reaching transitions in the whole society, Adv. Clim. Chang. Res. 12 (2) (2021) 281–286.
[8] V. Singh, P. Dixit, R. Venugopal, K.B. Venkatesh, Ore pretreatment methods for grinding: journey and prospects, Miner. Process. Extr. Metall. Rev. 40 (1) (2019) 1–15.
[9] H. Wei, S. Fengnian, Selective breakage of mineralised synthetic particles by high voltage pulses. Part 2: interactions between mineralised particles in a multiple-particle system, Miner. Eng. 146 (2020), 106149.
[10] S. Sen, Grinding of magnetite using a waterjet driven cavitation cell, Powder Technol. 297 (2016) 34–43.
[11] H. Kuyumcu, L. Rolf, Application of high-pressure waterjets for comminution, Int. J. Miner. Process. 74 (2004) S191–S198.
[12] I. Suzuki, Microbial leaching of metals from sulfide minerals, Biotechnol. Adv. 19 (2) (2001) 119–132.
[13] V. Singh, V. Saxena, R. Raj, R. Venugopal, Artificial weathering of coal to enhance milling performance, Fuel 142 (2015) 117–120.
[14] A. Swart, P. Mendonidis, Evaluating the effect of radio-frequency pre-treatment on granite rock samples for comminution purposes, Int. J. Miner. Process. 120 (2013) 1–7.
[15] A.J. Swart, Evaluating the effects of radio-frequency treatment on rock samples: Implications for rock comminution, in: Geochemistry-Earth's System Processes, IntechOpen, 2012.
[16] C.-G. Cho, H.-J. Ryoo, Design of compact solid-state modulator for high-power electromagnetic pulse generation, IEEE J. Emerg. Select. Topics Power Electron. 9 (5) (2021) 6059–6068.
[17] V. Singh, I.O. Samuelraj, R. Venugopal, G. Jagadeesh, P. Banerjee, Study the effect of electrical and mechanical shock loading on liberation and milling characteristics of mineral materials, Miner. Eng. 70 (2015) 207–216.
[18] K. Schönert, Breakage of spheres and circular discs, Powder Technol. 143 (2004) 2–18.
[19] G.H. Zhang, C. Feng, Y.B. Fan, S.H. Li, Preliminary study on application scope of new ore pulverizing technology, E3S Web Conf. 233 (2021) 01052–01057.
[20] Y.B. Fan, W.J. Duan, S.H. Li, J.Y. Qiao, Experiment on micron-sized particle production of iron ore by rapid unloading of liquid $CO_2$, Powder Technol. 327 (2018) 449–455.
[21] Y.B. Fan, J.Y. Qiao, S.H. Li, C. Feng, Micron-sized silicon carbide particle production via rapid unloading of high-pressure liquid $CO_2$, J. Aust. Ceram. Soc. 55 (2) (2019) 595–600.
[22] Y.B. Fan, J.Y. Qiao, S.H. Li, C. Feng, Micron-sized ore powder production by propulsion and rapid unloading of high-pressure gas, J. Aust. Ceram. Soc. 57 (5) (2021) 1489–1497.
[23] Ś. Grzegorz, M. Janusz, Forward and inverse analysis for particle size distribution measurements of disperse samples: a review, Measurement 187 (2022), 110256.
[24] P. Rosin, E. Rammler, The Laws of governing the fineness of powdered Coal, J. Inst. Fuel. 7 (1993) 29–36.
[25] R. Schuhmann Jr., Principles of comminution, I-size distribution and surface calculations, Am. Inst. Min. Met. Eng., Tech. Pub. 1189 (1940) 1–11.
[26] A. Macías-García, M.C.-C. Eduardo, M.A. Díaz-Díez, Application of the Rosin–Rammler and Gates–Gaudin–Schuhmann models to the particle size distribution analysis of agglomerated cork, Mater. Charact. 52 (2) (2004) 159–164.
[27] M. Ghambari, M. Emadi Shaibani, N. Eshraghi, Production of grey cast iron powder via target jet milling, Powder Technol. 221 (2012) 318–324.
[28] F. Gauss, Theory of the Motion of Heavenly Bodies Moving about the Sun in Conic Sections (English transl. by CH Davis), reprinted 1963, 1809.
[29] E. Platen, A generalized Taylor formula for solutions of stochastic equations, Sankhyā: Indian J. Stat. Series A (1982) 163–172.
[30] Z.M. Odibat, N.T. Shawagfeh, Generalized Taylor's formula, Appl. Math. Comput. 186 (1) (2007) 286–293.
[31] C. Kang, J. Tsutsumi, K. Oda, Effect of loading rate on modulus of elasticity and modulus of rupture in bending of wood, Bull. Kyushu Univ. Forests 71 (1994) 47–56.